Available online at www.sciencedirect.com
SCIENCE DIRECT
Journal of Photochemistry and Photobiology A: Chemistry 181 (2006) 166–173
Journal of Photochemistry and Photobiology A:Chemistry
www.elsevier.com/locate/jphotochem

Photovoltaic properties of ordered mesoporous silica thin film electrodes encapsulating titanium dioxide particles

William A. Adams [a], Martin G. Bakker [a,*], Terence I. Quickenden [b]

[a] *Department of Chemistry, The University of Alabama, Tuscaloosa, AL 35487-0336, USA*
[b] *School of Biomedical, Biomolecular and Chemical Sciences, The University of Western Australia, Crawley, WA 6009, Australia*

Received 29 September 2005; received in revised form 19 November 2005; accepted 21 November 2005
Available online 20 January 2006

Dedicated to Terence Ivan Quickenden (1938–2005).

Abstract

SBA-15 mesoporous silica thin films encapsulating Degussa P-25 TiO_2 particles were synthesized using a block copolymer templating method. The films were dip-coated onto ITO conducting glass substrates to allow for photovoltaic analysis. Structural characterization of the films was performed using X-ray diffraction (XRD) and transmission electron microscopy (TEM). The electrodes were placed in photovoltaic cells and irradiated with long wavelength UV (∼365 nm) radiation. Photovoltaic efficiencies were determined to be in the range 8.0×10^{-4} to 0.26%. An increase in efficiency of approximately 44% was found for mesoporous silica samples encapsulating TiO_2 particles over non-porous silica films containing TiO_2.

Keywords: Titanium dioxide; Mesoporous silica films; Photovoltaics; Photoelectrochemical cell; Photovoltaic efficiency

1. Introduction

Titanium dioxide (TiO_2) has been of interest for many potential applications due to its high photocatalytic activity compared with other semiconductors. While undergoing photolysis, TiO_2 has been shown to effectively photodegrade organic wastes for water remediation [1–3] and has been shown to be potentially applicable for photovoltaic purposes [4–7].

A considerable amount of research has examined the use of TiO_2 in the field of photovoltaics as a substitute for silicon in solar cells [8–18]. These solar cells typically use a dye sensitizer in order to inject electrons into the conduction band of the semiconductor, thereby decreasing the band gap energy, and so allowing solar radiation to drive charge transfer. Gratzel and coworkers have shown that these TiO_2 dye-sensitized solar cells can provide efficiencies above 10% [11,14–17], which is comparable to crystalline silicon solar cells. Other semiconductors, such as zinc oxide and tin oxide, have been examined for their photovoltaic properties in solar cells [19–22].

It has been shown that mixed phase titania catalysts are more photoactive than the pure phase catalysts [23]. Degussa P-25 TiO_2 is a highly photoactive form of TiO_2 composed of 20–30% rutile and 70–80% anatase TiO_2. The particles range in size from 12 to 20 nm. Titanium dioxide has a band gap of 3.0–3.2 eV, which corresponds to a wavelength of 380–400 nm. Therefore, any wavelength below 380 nm can excite electrons in the valence band of the semiconductor to the conduction band, allowing for charge transfer. There has been interest in studying the effect of incorporating multiple forms of titania with mesoporous silica for various applications [24–32]. However, many of these methods involve the use of less photoactive forms of titania, such as anatase, or only apply the particles to the surface of the mesoporous silica which can limit the overall density obtainable for the photocatalyst and which has the potential for significant particle loss because of the absence of covalent bonding. The encapsulation of a highly photoactive P-25 titanium dioxide within a thin film of mesoporous silica with a 2–10 nm pore size could provide advantages, which will be discussed. To the best of our knowledge, there are no previous reports of incorporation of photoactive nanoparticles into an ordered mesoporous matrix for photovoltaic applications.

* Corresponding author. Tel.: +1 205 348 9116; fax: +1 205 348 9104.
E-mail address: Bakker@bama.ua.edu (M.G. Bakker).

1010-6030/$ – see front matter © 2006 Elsevier B.V. All rights reserved.
doi:10.1016/j.jphotochem.2005.11.020

The combination of surfactants and polymers with sol–gel methods to synthesize silica has been shown to be a useful means to produce ordered mesoporous silica thin films [33–38]. SBA-15 is a form of mesoporous silica (SiO_x) synthesized using a sol–gel method combining a silicon alkoxide with a block co-polymer to act as a template for the formation of hexagonally ordered arrays of pores [35,36,39]. In this process, the silicon alkoxide undergoes hydrolysis to produce silicic acid and oligomers of silicic acid. After hydrolysis, condensation will occur. It is necessary for the pH to be low in order for condensation to occur slowly. The slow rate of condensation allows time for the templating polymer to organize into hydrophobic and hydrophilic domains. The silicate polymers solubilize within the hydrophilic domains of the polymer and condense. Solvents are added to the silicate/polymer solution to spread the solution and aid in slowing the condensation. The pores within the silica will often align themselves in a thin film parallel to the surface of the substrate due to shear forces applied during preparation and inherent interface effects [35,36]. Thin film templated mesoporous silica is expected to allow faster counterion diffusion and to produce an increase in surface area compared with non-porous thin films.

This work focuses on samples with various amounts of Degussa P-25 TiO_2 encapsulated in SBA-15 mesoporous silica thin film matrices on ITO glass substrates and their application to photoelectrochemical studies. Of particular interest is the photovoltaic comparison of electrodes containing porous and non-porous films of silica encapsulating P-25 TiO_2 particles. The addition of an ordered porous network encapsulating highly photoactive titania should allow for faster diffusion of counterions in solutions and an increased photoactive surface area available for a more efficient photoconversion compared to non-porous films of pure titania.

The setup of the photochemical cell used in this study follows the photosynthetic cell type, which would involve photovoltage production due to electron–hole migration with a water cleavage mechanism completing the circuit. With this type of photovoltaic device, the semiconductor, when irradiated, produces electron–hole pairs. The electrodes in this study are irradiated using a UV light source. This allows for charge transfer to occur under direct photolysis conditions without the use of a dye sensitizer. The use of a dye sensitizer would be expected to allow the use of longer wavelengths, such as visible radiation. However, this would seriously complicate interpretation of the data since the dyes used would be expected to partition between the mesoporous silica and the TiO_2 particles. Hence, it would not be possible to evaluate the effect of using a mesoporous matrix. The electrons generated within the semiconductor due to the UV irradiation tend to migrate to the conducting substrate, while the positively charged holes tend to migrate to the surface of the semiconductor. The electrons then travel through the external circuit to the counter electrode. In order to complete the circuit, we would expect that water is oxidized at the semiconductor surface to produce oxygen and reduced at the counter-electrode to produce hydrogen [18,40]. The experimental method used in this study follows photoelectrochemical analysis methods reported by Quickenden et al. [41,42]. Structural characterization of the films was carried out using X-ray diffraction (XRD) and transmission electron microscopy (TEM) to establish the formation of the mesoporous silica and to examine the incorporation of the P-25 TiO_2 particles in the mesoporous silica films. The photovoltaic efficiency was determined for all samples using the power produced by the various electrodes and compared with TEM and XRD data.

2. Experimental

2.1. Materials

For the SBA-15 synthesis, tetraethyl orthosilicate (TEOS, 98% Aldrich), poly(ethylene oxide)–poly(propylene oxide)–poly(ethylene oxide) block copolymer (Pluronic® 123, BASF), and P-25 titanium dioxide (Degussa) were used as received. Concentrated HCl (Fisher) in deionized water (pH 1–2) and 100% ethanol (Aaper) were available.

For the photovoltaic measurements, potassium chloride (ACS reagent, Sigma–Aldrich) was used as received. Standard indium tin oxide (ITO) glass plates were cut using a diamond wheel and cleaned using an acid/base wash. Reticulated vitreous carbon wafers (ERG) with an area of 5.25 in^2 (33.87 cm^2) were used as counterelectrodes.

2.2. Instrumentation

X-Ray diffraction data for film characterization was collected on a Philips X-ray diffractometer using Cu Kα radiation ($\lambda = 1.5406$ Å). Samples of the thin films were scraped off the ITO glass with a razor blade and washed onto a holey carbon TEM grid using ethanol as the solvent and examined by transmission electron microscopy using a JEOL 2000F transmission electron microscope operating at 200 kV. The digital images were acquired and processed using a Gatan MultiScan 600CW CCD. Characterization by UV–vis spectroscopy was carried out using a Cary 50 scan UV–vis spectrophotometer.

The film thicknesses were determined using an FEI Quanta 3D duel beam scanning electron microscope (SEM). All photovoltaic measurements were collected using a Cole-Parmer Instrument Company model 8373-10 chart recorder. The lamp used for sample irradiations was a Spectroline Longwave 365 nm UV lamp.

2.3. Photoelectrochemical cell

The photoelectrochemical cell was setup using mesoporous silica thin films encapsulating TiO_2 particles coated on indium tin oxide (ITO) glass as the working electrode, and a reticulated vitreous carbon rectangle as the counter electrode. The electrodes were placed in a beaker and were immersed in a 0.1 M KCl solution at pH 3.5, so that 1.378 in (3.5 cm) of the electrode was immersed in solution. This provided a total area of 7.0 cm^2 for all photovoltaic measurements. The electrodes were spaced 0.75 in (1.905 cm) apart. The cell was then connected in parallel with a decade resistance box and the chart recorder.

A Woods glass filter was placed between the lamp and the photoelectrochemical cell to allow for UV light to pass while blocking visible light. The lamp used was placed 2.598 in (6.6 cm) from the working electrode at the center of the long axis of the lamp.

2.4. Synthesis of SBA 15/P-25 thin films on ITO glass

The synthesis of SBA-15 is a sol–gel process and the procedure is outlined by Alberius et al. [35]. The synthesis of the SBA-15/P-25 thin films was carried out using the procedure described in our earlier work [39]. The amount of P-25 included in the precursor solution, referred to as the loading, was varied between 1 and 70 wt.% of the total weight of silica and P-25. The material was coated using a dip-coater at a rate of 1 mm/s onto various substrates to form thin films. The substrates included glass slides for XRD analysis and 2 cm × 5 cm (0.787 in. × 3.937 in.) ITO glass slides for the photovoltaic experiments.

3. Results and discussion

3.1. Characterization

3.1.1. XRD

X-Ray diffraction over the range 0–5° was used to detect the presence of an ordered structure within the SBA-15/P-25 thin films. A detailed description of this method can be found in Adams et al. [39].

An XRD spectrum was taken for each of the thin film samples ranging from 1 to 70 wt.% P-25 TiO_2 in mesoporous silica. Fig. 1 shows a typical XRD spectrum from a 10 wt.% TiO_2 in mesoporous silica thin film. Peaks at 1.52° and 2.93° are visible, corresponding to the [1 0 0] and [2 0 0] lattice peaks, respectively, consistent with hexagonal ordering [35,36]. Fig. 2 shows the *d*-spacing calculated from the position of the [1 0 0] peak as a function of wt.%. The figure shows that the *d*-spacing increases with increasing wt.%. The plot was well fit to an exponential function, however, this is purely empirical and not based on any particular model. The increase in *d*-spacing indicates that the incorporation of P-25 TiO_2 particles does affect the pore to pore spacing within the mesoporous silica matrix. As the concentration of particles increases, the distance from the center of one pore to the center of the next increases.

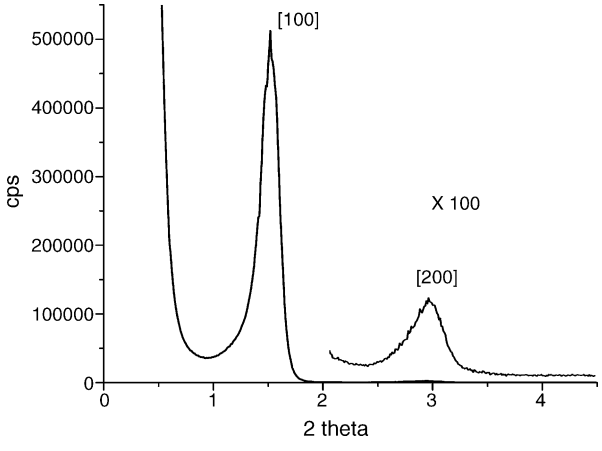

Fig. 1. X-ray diffraction pattern of 10 wt.% P-25 TiO_2 encapsulated in mesoporous silica thin film showing the crystal lattice peaks.

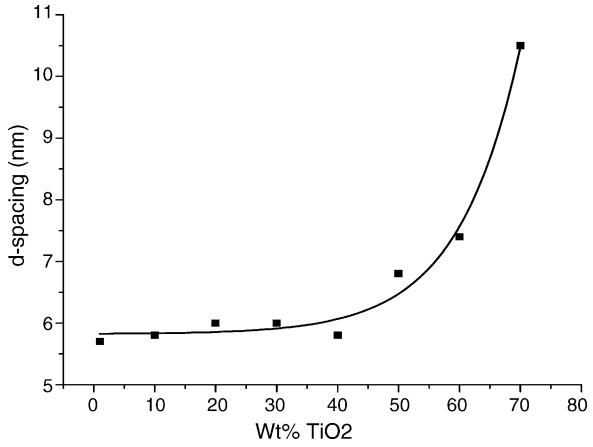

Fig. 2. Plot of *d*-spacing determined by X-ray diffraction vs. wt.% P-25 TiO2 encapsulated in mesoporous silica thin films. The data is fit as an exponential to guide the eye.

3.1.2. TEM

Thin films of SBA-15 encapsulating varying amounts of P-25 TiO_2 (1–70 wt.%) were examined using transmission electron microscopy. In Fig. 3, pores within the silica and the P-25 TiO_2 particles can be seen. Aggregation among the TiO_2 particles is evident as clumps of particles of various sizes, with the overall size and number of clumps increasing as the concentration of particles increases. The particle aggregations are distributed over the entire area of the thin film. It appears that the addition of the P-25 particles does have some effect on the size of the hexagonally ordered domains of pores within the silica, which are observed to decrease in size with increasing TiO_2. The presence of the TiO_2 particles makes it difficult to determine the degree of ordering within the higher TiO_2 load samples, and so it is not possible to determine if the degree of ordering also decreases. The decreasing domain size is consistent with XRD data that shows a trend in decreasing peak intensity as the TiO_2 particle concentration increases. The inclusion of the particles does not seem to prevent the formation of pores, although it does become more difficult to observe the presence of the pores in the TEM images, as the concentration of TiO_2 increases. In the TEM images, it is evident that the pores generally appear to terminate at the surface of the TiO_2 particles. However, it can also be seen that some of the pores bend around TiO_2 particles.

3.1.3. Film thickness versus titania loading

An environmental scanning electron microscope (ESEM) was used to examine cross-sections of mesoporous silica thin films encapsulating various amounts of TiO_2 particles in order to determine the film thicknesses. The results of the analysis can be seen in Fig. 4. The plot shows an increase in film thickness as the concentration of P-25 TiO_2 particles increases. This increase in thickness is likely due to the increase in P-25 TiO_2 particles causing changes in the viscosity of the solution, thereby changing the coating characteristics of the films during the sample

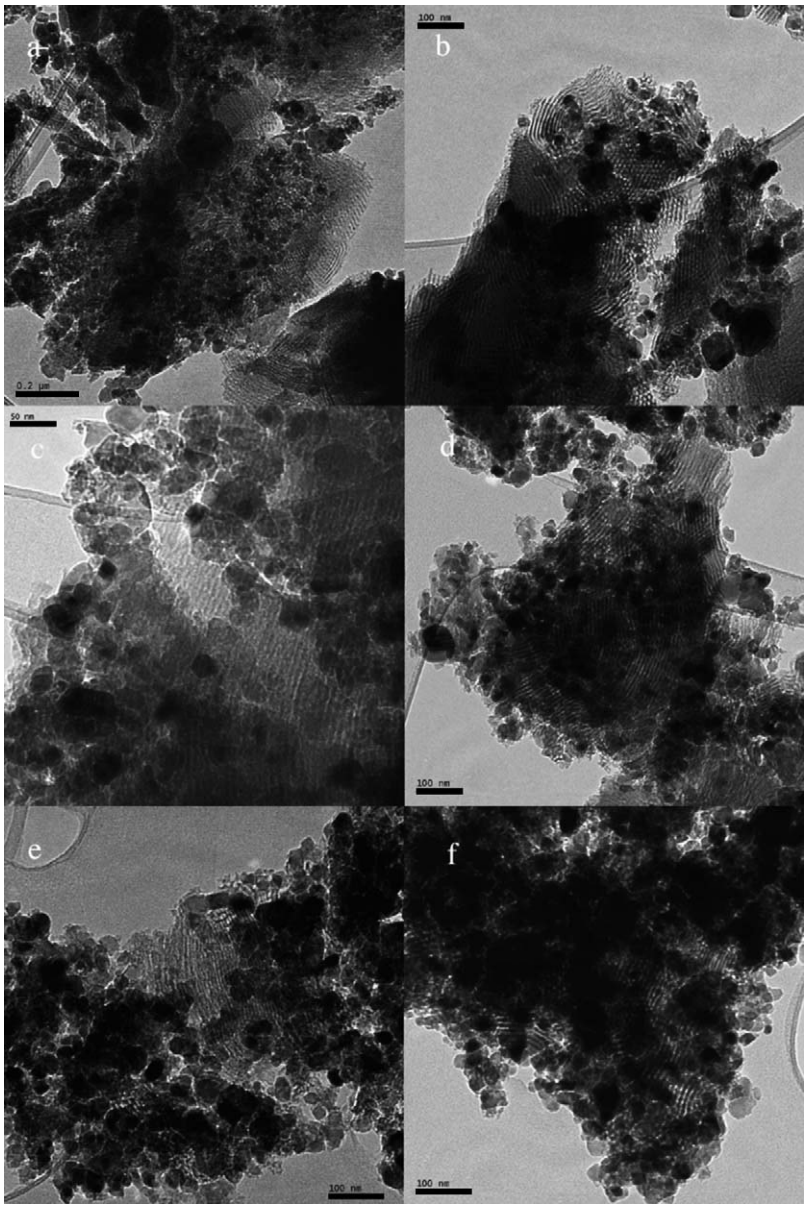

Fig. 3. Transmission electron microscope images of (a) 10 wt.%; (b) 20 wt.%; (c) 30 wt.%; (d) 50 wt.%; (e) 60 wt.%; and (f) concentration of particles 70 wt.% P-25 TiO_2 encapsulated in mesoporous silica thin films.

preparation. As seen in the TEM images, the increased loading of TiO_2 particles causes an increase in the aggregation of particles. The ESEM images suggest that this is accompanied by an increase in surface roughness. The presence of thicker films could adversely effect the electron conduction by increasing the distance the electron must travel to reach the conductor. Thicker films might also increase the amount of light absorbed within the electrode, however, UV absorption measurements indicate that by 12 wt.% loading only a relatively small (8%) portion of 365 nm light is transmitted by the electrode.

3.2. Photovoltaic experiments

3.2.1. Woods glass and UV lamp profile

The spectral profile for the UV lamp used in the experiment with and without the Woods glass filter can be seen in Fig. 5. The Woods glass was used to prevent any visible light from interfering with the photovoltaic measurements, as Woods glass is a commercially available UV pass/visible block filter. The spectral range for the experiment was approximately 300–410 nm, with the maximum intensity at a wavelength of 352 nm. All photovoltaic measurements for the determination of photovoltaic efficiency were analyzed using the Woods glass filter.

The total integrated power measured for the lamp without any filters was 4941 $\mu W/cm^2$. The measurements were performed using a reference ultraviolet spectroradiometer. The input optic was a 15.24 cm (6 in.) spectral on integrating sphere with a 2.54 cm (1 in.) diameter input port. The measurements were at 1 nm resolution.

The total integrated power of the lamp using the Woods glass filter was determined to be 3078 $\mu W/cm^2$.

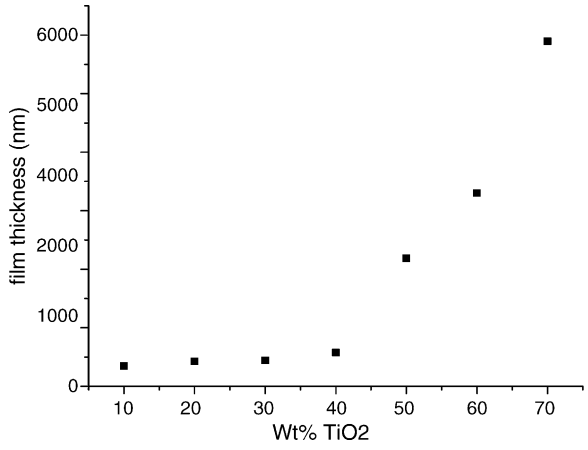

Fig. 4. Plot of film thickness of mesoporous silica encapsulating P-25 TiO_2 vs. wt.% P-25 TiO_2 encapsulated in mesoporous silica thin films.

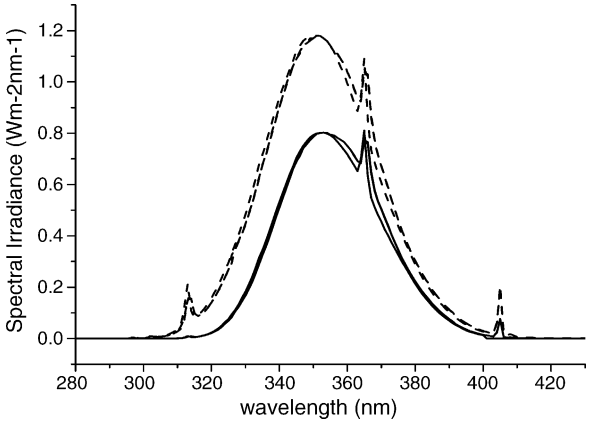

Fig. 5. Sperctral profile of UV lamp with a Wood's glass filter (—) and without a filter (– – –).

3.2.2. *Photovoltaic efficiency*

The potential was measured for each of the electrodes containing varying loadings of P-25 TiO_2 encapsulated in mesoporous silica thin films. Initially, the potential dropped in intensity immediately after reaching a maximum potential and so each sample was allowed to come to equilibrium. The maximum potential was taken from the point at which the cell potential stabilized. The drop in potential increased in rate and magnitude as the power output and TiO_2 loading of the different electrodes increased. It is believed that this drop could be due to surface charge effects caused by accumulation of positively charged holes at the surface of the TiO_2 particles. The potential stabilization would be due to an equilibrium occurring between the rate of transfer of holes to the surface and the rate of electron percolation through the TiO_2. From the stabilized potential values, the maximum power output for each of the electrodes was calculated using a plot of the potential difference versus the current applied to the cell (V versus I). Fig. 6 shows the voltage versus current curves of three different electrodes of varying wt.% of TiO_2 encapsulated in mesoporous silica. From these plots, the point at which a rectangle achieves maximum area is calculated. This point is the maximum power output of the electrode and

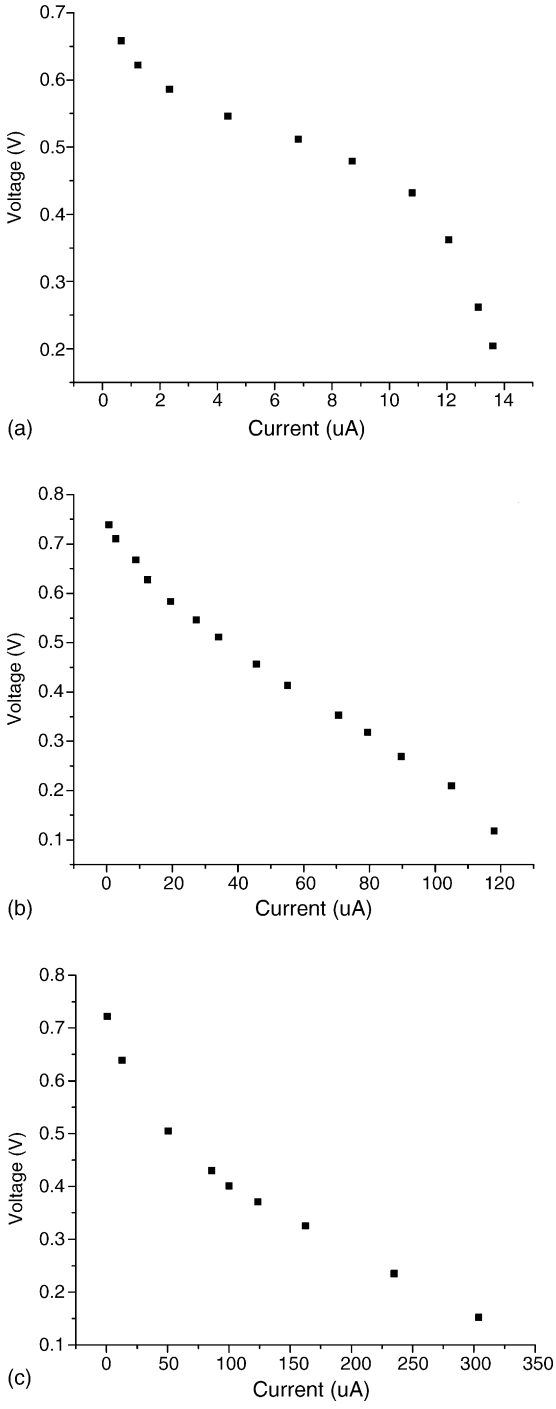

Fig. 6. Voltage vs. current curve for (a) 10 wt.%; (b) 40 wt.%; and (c) 70 wt.% P-25 TiO_2 encapsulated in mesoporous silica.

can be determined graphically by a plot of the potential squared versus the current applied to the cell (V^2 versus I).

In order to determine the photovoltaic efficiency of the cell, the maximum power output of the cell is divided by the maximum power input from the lamp. The overall power of the lamp was determined to be 3078 $\mu W/cm^2$. The power input from the lamp is distributed over the entire irradiated surface of the electrode, 7.0 cm^2. Therefore, the total power input for the electrode is 215,48 μW. An initial dark voltage of approximately 50 mV is

Table 1
The effect of P-25 TiO_2 wt.% on the maximum power output and photoefficiency

Weight % P-25 TiO_2	Maximum power output (μW)	Photovoltaic efficiency (%)
1	0.18	8.0×10^{-4}
10	4.14	1.9×10^{-2}
20	6.63	3.1×10^{-2}
30	11.5	5.3×10^{-2}
40	24.89	0.12
50	38.28	0.18
60	44.65	0.21
70	55.94	0.26

observed during the setup of the photovoltaic cell. However, the dark voltage is checked and zeroed out at the beginning and end of each experimental run. The photovoltaic efficiencies for the varying loading of P-25 TiO_2 can be calculated and are shown in Table 1.

A plot of the power output versus wt.% can be seen in Fig. 7. There appears to be a nonlinear trend as the P-25 loading increases, the power output increases more than proportionally. There was no clear correlation between *d*-spacing versus TiO_2 wt.% and power output versus TiO_2 wt.%, although, both *d*-spacing and power increased with increased TiO_2 loading.

Studies of the photoactivity of P-25 TiO_2 particles encapsulated in mesoporous silica found that sonication decreased particle aggregation and increased photoactivity by 4.2% (Adams et al., 2003, unpublished data). Accordingly, the effect of sonication on the photovoltaic properties was assessed.

Several samples were prepared in which the sol–gel solutions used to make the thin films were sonicated for 1 h immediately after adding the P-25 TiO_2 particles. All other steps in the synthesis were followed in the same manner as the samples not sonicated and subsequently analyzed in the same manner as well. The sonicated electrodes were compared with electrodes not sonicated, and a difference of less than 2% was observed between the two samples. Therefore, it appears that if the sonication was producing better distribution of the P-25 TiO_2 particles, the resulting power increase is not significant.

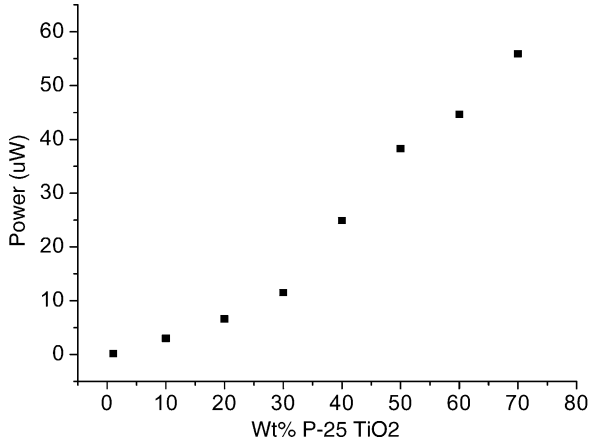

Fig. 7. The effect of P-25 TiO_2 wt.% in mesoporous silica thin film on the power output of the photovoltaic cell.

3.2.3. Correlation of samples using mesoporous and non-porous samples

The potential and power measurements were conducted using varying loadings of P-25 TiO_2 encapsulated in non-porous silica. Three loading values were selected for the comparison, 10, 40, and 70 wt.%. This data set provided a survey range for the previous mesoporous silica power measurement experiments.

The power output for each of the non-porous silica samples was compared with the mesoporous silica samples. It was found that there was not a strong correlation between improvement in efficiency and wt.% among the samples, but the average increase in efficiency due to using mesoporous silica was $44 \pm 38\%$. The error included is the 95% confidence limit, and although high, does indicate that there is a significant increase in efficiency due to the addition of mesoporosity.

3.2.4. Neutral density filter saturation analysis

Due to the high total energy of the UV lamp, it was necessary to ensure that the electrode was not being saturated by the amount of power being input into the photochemical cell from the UV lamp. To measure this, a neutral density filter determined to transmit 42.3% of the light was placed between the lamp and the photovoltaic cell in order to allow a known amount of light able to reach the cell.

A 40 wt.% P-25 TiO_2 encapsulated in a mesoporous silica thin film electrode was examined and analyzed using our standard procedure while using the neutral density filter. The total power output of the filtered system was found to be 41.7% of the non-filtered system. The difference between the amount of light being transmitted and the power drop caused by the filtered light was 1.5%. Therefore, it is clear that the photoelectrode is not being saturated.

4. Conclusions

SBA-15 thin films encapsulating varying loadings of P-25 titanium dioxide particles were synthesized and dip-coated onto ITO glass electrodes for photovoltaic analysis. The films were shown to be ordered and mesoporous using XRD and TEM techniques. Photovoltaic data showed that the mesoporous thin films achieved an overall photovoltaic efficiency range of 8.0×10^{-4} to 0.26% under direct photolysis conditions. It was also shown that there was a significant ($44 \pm 38\%$) increase in photovoltaic efficiency for mesoporous silica compared to non-porous silica media.

Mesoporous silica was chosen as the matrix due to the ease with which it can be synthesized. It is, however, an insulator. This may be why only modest increases in power output are seen in comparison with using a non-porous silica matrix. However, it is possible that by encapsulating TiO_2 particles into conducting mesoporous matrixes, such as SnO_2, higher power efficiency could be produced. Likewise, by altering the encapsulated particle, the power efficiency and light harvesting properties of the matrix could be tuned. We believe that by incorporating nanoparticles in a mesoporous matrix, we have developed a system with significantly increased flexibility.

Acknowledgements

The authors would like to thank the NSF-EAPSI (WA) program for support. Measurements obtained by Jason Manning on The University of Alabama's FIB/ESEM and Daryl Myers of NREL (spectral profile of the lamp) are very much appreciated. The authors are also thankful for the gifts of P-25 TiO_2 from Degussa and P123 from BASF. The authors also appreciate access to instruments and facilities in the MINT Center and the MRSEC at The University of Alabama under grant DMR-0213985. The authors would also like to thank NASA for TEM technical support, the NASA Space Act Agreement, and the Alabama Space Grant Consortium.

References

[1] O. Legrini, E. Oliveros, A.M. Braun, Photochemical processes for water treatment, Chem. Rev. 93 (1993) 671–698.
[2] M.R. Hoffmann, S.T. Martin, W. Choi, D.W. Bahnemann, Environmental applications of semiconductor photocatalysis, Chem. Rev. 95 (1995) 69–96.
[3] M.A. Fox, M.T. Dulay, Heterogeneous photocatalysis, Chem. Rev. 93 (1993) 341–357.
[4] F. Campus, P. Bonhote, S. Heinen, L. Walder, Electrochromic devices based on surface-modified nanocrystalline TiO_2 thin-film electrodes, Sol. Energy Mater. Sol. Cells 56 (1999) 281–297.
[5] J.E. Moser, P. Bonnate, M. Gratzel, Molecular photovoltaics, Coord. Chem. Rev. 17 (1998) 245–250.
[6] A. Hagfeldt, M. Gratzel, Light-Induced reactions in nanocrystalline systems, Chem. Rev. 95 (1995) 49–68.
[7] P.V. Kamat, Photochemistry on nonreactive and reactive (semiconductor) surfaces, Chem. Rev. 93 (1993) 267–300.
[8] Y.-Q. Wang, S.-G. Chen, X.-H. Tang, O. Palchik, A. Zaban, Y. Koltypin, A. Gedanken, Mesoporous titanium dioxide: sonochemical synthesis and application in dye-sensitized solar cells, J. Mater. Chem. 11 (2001) 521–526.
[9] A.J. Frank, N. Kopidakis, J. van de Lagemaat, Electrons in nanostructured TiO_2 solar cells: transport, recombination, and photovoltaic properties, Coord. Chem. Rev. 248 (2004) 1165–1179.
[10] M. Gratzel, Sol–gel processed TiO_2 films for photovoltaic applications, J. Sol–Gel Sci. Technol. 22 (2001) 7–13.
[11] B. O'Regan, M. Gratzel, A low-cost, high-efficiency solar cell based on dye-sensitized colloidal, Nature 353 (1991) 737–740.
[12] A.J. McEvoy, M. Gratzel, Sensitisation in photochemistry and photovoltaics, Sol. Energy Mater. Sol. Cells 32 (1994) 221–227.
[13] M. Adachi, Y. Murata, I. Okada, S. Yoshikawa, Formation of titania nanotubes and applications for dye-sensitized solar cells, J. Electrochem. Soc. 150 (2003) G488–G493.
[14] N. Vlachopoulos, P. Liska, J. Augustynski, M. Gratzel, Very efficient visible light energy harvesting and conversion by spectral sensitization of high surface area polycrystalline titanium dioxide films, J. Am. Chem. Soc. 110 (1988) 1216–1220.
[15] M.K. Nazeeruddin, A. Kay, I. Rodicio, R. Humphry-Baker, E. Muller, P. Liska, N. Vlachopoulos, M. Gratzel, Conversion of light to electricity by *cis*-X2Bis(2,2′-bipyridal-4,4′-dicarboxylate)ruthenium(II) charge transfer sensitizers ($X = CL^-$, Br^-, I^-, CN^-, and SCN^-) on nanocrystalline TiO_2 electrodes, J. Am. Chem. Soc. 115 (1993) 6382–6390.
[16] M. Gratzel, Dye-sensitized solar cells, J. Photochem. Photobiol. C 4 (2003) 145–153.
[17] M. Gratzel, Conversion of sunlight to electric power by nanocrystalline dye-sensitized solar cells, J. Photochem. Photobiol. A164 (2004) 3–14.
[18] M. Gratzel, Photoelectrochemical cells, Nature 414 (2001) 338–344.
[19] Z.-S. Wang, C.-H. Huang, Y.-Y. Huang, Y.-J. Hou, P.-H. Xie, B.-W. Zhang, H.-M. Cheng, A highly efficient solar cell made from a dye-modified ZnO-covered TiO_2 nanoporous electrode, Chem. Mater. 13 (2001) 678–682.
[20] D.D. Hawn, N.R. Armstrong, Electrochemical adsorption and covalent attachment of erythrosin to modified tin dioxide electrodes and measurement of the photocurrent to visible wavelength light, J. Phys. Chem. 82 (1978) 1288–1295.
[21] S. Ito, Y. Makari, Y. Kitamura, S. Yanagida, Fabrication and characterization of mesoporous SnO_2/ZnO_2 composite electrodes for efficient dye solar cells, J. Mater. Chem. 14 (2004) 385–390.
[22] K.M.P. Bandaranayake, M.K.I. Senevirathna, P.M.G.M.P. Weligamuwa, K. Tennakone, Dye-sensitized solar cells made from nanocrystalline TiO_2 films coated with outer layers of different oxide materials, Coord. Chem. Rev. 248 (2004) 1277–1281.
[23] R.R. Basca, J. Kiwi, Effect of rutile phase on the photocatalytic properties of nanocrystalline titania during the degradation of *p*-coumaric acid, Appl. Catal. B 16 (1998) 19–29.
[24] L.J. Alemany, M.A. Baneres, E. Pardo, F. Martin, M. Galan-Fereres, J.M. Blasco, Photodegradation of phenol in water using silica-supported titania catalysts, Appl. Catal. B 13 (1997) 289–297.
[25] B.J. Aronson, C.F. Blanford, A. Stein, Solution-phase grafting of titanium dioxide onto the pore surface of mesoporous silicates: synthesis and structural characterization, Chem. Mater. 9 (1997) 2842–2851.
[26] Q. Dai, N. He, K. Weng, B. Lin, Z. Lu, C. Yuan, Enhanced photocatalytic activity of titanium dioxide supported on hexagonal mesoporous silica at lower coverage, J. Inclusion Phenom. Macrocyclic Chem. 35 (1999) 11–21.
[27] Y. Xu, C.H. Langford, Enhanced photoactivity of a titanium (IV) oxide supported on ZSM5 and zeolite A at low coverage, J. Phys. Chem. 99 (1995) 11501–11507.
[28] Y. Xu, C.H. Langford, Photoactivity of titanium dioxide supported on MCM41, zeolite X, and zeolite Y, J. Phys. Chem. 101 (1997) 3115–3121.
[29] S.W. Ahn, L. Kevan, Photoionization of titanium dioxide particles incorporated into silica gels of different pore sizes, J. Chem. Soc., Faraday Trans. 94 (1998) 3147–3153.
[30] A.A. Belhekar, S.V. Awate, R. Anand, Photocatalytic activity of titania modified mesoporous silica for pollution control, Catal. Commun. 3 (2002) 453–458.
[31] Z. Luan, E.M. Maes, P.A.W. van der Heide, D. Zhao, R.S. Czernuszewicz, L. Kevan, Incorporation of titanium into mesoporous silica molecular sieve SBA-15, Chem. Mater. 11 (1999) 3680–3686.
[32] Y.-H. Hsien, C.-F. Chang, Y.-H. Chen, S. Cheng, Photodegradation of aromatic pollutants in water over TiO_2 supported on molecular sieves, Appl. Catal. B 31 (2001) 241–249.
[33] A. Gibaud, D. Grosso, B. Smarsly, A. Baptiste, J.F. Bardeau, F. Babonneau, D.A. Doshi, Z. Chen, C.J. Brinker, C. Sanchez, Evaporation-controlled self-assembly of silica surfactant mesophases, J. Phys. Chem. B 107 (2003) 6114–6118.
[34] C.J. Brinker, G.W. Scherer, Hydrolysis and Condensation of Silicon Alkoxides, in Sol-Gel Science: The Physics and Chemistry of Sol-Gel Processing, Academic Press Inc., Boston/San Diego/New York/London/Sydney/Tokyo/Toronto, 1990, p. 180.
[35] P.C.A. Alberius, K.L. Frindell, R.C. Hayward, E.J. Kramer, G.D. Stucky, B.F. Chmelka, General predictive synthesis of cubic, hexagonal, and lamellar silica and titania mesostructured thin films, Chem. Mater. 14 (2002) 3284–3294.
[36] D. Zhao, P. Yang, N. Melosh, J. Feng, B.F. Chmelka, G.D. Stucky, Continuous mesoporous silica films with highly ordered large pore structures, Adv. Mater. 10 (1998) 1380–1385.
[37] J.S. Beck, J.C. Vartulli, W.J. Roth, M.E. Leonowicz, C.T. Kresge, K.D. Schmitt, C.T.-W. Chu, D.H. Olson, E.W. Sheppard, S.B. McCullen, J.B. Higgins, J.L. Schlenker, A new family of mesoporous molecular sieves prepared with liquid crystal templates, J. Am. Chem. Soc. 114 (1992) 10834–10843.
[38] C.T. Kresge, M.E. Leonowicz, W.J. Roth, J.C. Vartulli, J.S. Beck, Ordered mesoporous molecular sieves synthesized by a liquid-crystal template mechanism, Nature 359 (1992) 710–712.

[39] W.A. Adams, M.G. Bakker, T. Macias, I.A. Jefcoat, Synthesis and characterization of mesoporous silica films encapsulating titanium dioxide particles. Photodegradation of 2,4-dichlorophenol, J. Hazard. Mater. B112 (2004) 253–259.

[40] A. Fujishima, K. Honda, Electrochemical photolysis of water at a semiconductor electrode, Nature 238 (1972) 37–38.

[41] T.I. Quickenden, G.K. Yim, Measured dependence of photovoltage on irradiance in the gold-rhodamine B photoelectrochemical cell, J. Phys. Chem. 84 (1980) 670–674.

[42] T.I. Quickenden, R.L. Bassett, Electrodic dye layers in the gold-rhodamine B photoelectrochemical cell, J. Phys. Chem. 85 (1981) 2232–2238.